parameter hidden in the copper oxide phase diagram. Recent angle-resolved photoemission spectroscopy (ARPES) measurements indicate a possible broken time-reversal symmetry in the pseudogap regime, implying that it is a real thermodynamic phase[20]; this must be established by further experiments. This ARPES experiment has been interpreted as support for a phase with circulating currents[5]. Indeed, several theoretical studies on hole-doped high-T_c superconductors have highlighted the possibility of a quantum critical point in the phase diagram involving the existence of a second order parameter[1,5–7,21–23]. It is already well known that antiferromagnetic Néel order and a charge/spin (stripe) density wave exist in the copper oxide phase diagram. In addition, the possibility of *d*-density wave[7] (staggered flux) order and $d_{x^2-y^2} + id_{xy}$ or $d_{x^2-y^2} + is$ superconductivity has been discussed in detail. Recent neutron-scattering experiments on $La_{2-x}Sr_xCuO_4$ (ref. 24) and $YBa_2Cu_3O_{6.6}$ (ref. 25) have revealed enhanced antiferromagnetic correlations in the underdoped superconducting region. Another example of hidden order was found in the heavy fermion metal URu_2Si_2 (ref. 26). In the phase diagram suggested here for electron-doped high-T_c superconductors, there (co)exist at least two competing order parameters. A small applied magnetic field couples only to the superconducting order parameter, suppressing it completely at H_{c2} leaving the pseudogap-related order parameter at a finite value, as predicted recently for a *d*-density-wave ordered state[27]. This excludes the possibility that the pseudogap regime is related to a second superconducting order parameter with different symmetry[28]. Owing to the competition of the two order parameters, the magnetic field needed to destroy superconductivity can indeed be smaller than H_{c2} because of the additional suppression of superconductivity by the competing order. Strong interactions between the two order parameters can result in even more complicated phase diagrams with more phases than shown in Fig. 4. The identification of the possible order in the pseudogap phase is one of the most prominent questions in the field of high-T_c superconductivity. Any suggested order should be consistent with the observations that the pseudogap coexists with superconductivity and is essentially unchanged by a large applied external field. In particular, these constraints exclude the physical picture of precursor superconductivity. □

Received 10 July 2002; accepted 7 February 2003; doi:10.1038/nature01488.

1. Tallon, J. L. & Loram, J. W. The doping dependence of T^*—what is the real high-T_c phase diagram? *Physica C* **349,** 53–68 (2001).
2. Timusk, T. & Statt, B. The pseudogap in high-temperature superconductors: an experimental survey. *Rep. Prog. Phys.* **62,** 61–122 (1999).
3. Emery, V. J. & Kivelson, S. A. Importance of phase fluctuations in superconductors with small superfluid density. *Nature* **374,** 434–437 (1995).
4. Xu, Z. A., Ong, N. P., Wang, Y., Kakeshita, T. & Uchida, S. Vortex-like excitations and the onset of superconducting phase fluctuation in underdoped $La_{2-x}Sr_xCuO_4$. *Nature* **406,** 486–488 (2000).
5. Varma, C. M. Pseudogap phase and the quantum-critical point in copper-oxide metals. *Phys. Rev. Lett.* **83,** 3538–3541 (1999).
6. Sachdev, S. Quantum criticality: competing ground states in low dimensions. *Science* **288,** 475–480 (2000).
7. Chakravarty, S., Laughlin, R. B., Morr, D. K. & Nayak, C. Hidden order in the cuprates. *Phys. Rev. B* **63,** 094503 (2001).
8. Naito, M. & Hepp, M. Superconducting T'-$La_{2-x}Ce_xCuO_4$ films grown by molecular beam epitaxy. *Jpn. J. Appl. Phys.* **39,** L485–L487 (2000).
9. Kleefisch, S. *et al.* Possible pseudogap behavior of electron-doped high-temperature superconductors. *Phys. Rev. B* **63,** R100507 (2001).
10. Mannhart, J. *et al.* Generation of magnetic flux by single grain boundaries of $YBa_2Cu_3O_{7-x}$. *Phys. Rev. Lett.* **77,** 2782–2785 (1996).
11. Onose, Y., Taguchi, Y., Ishizaka, K. & Tokura, Y. Doping dependence of pseudogap and related charge dynamics in $Nd_{2-x}Ce_xCuO_4$. *Phys. Rev. Lett.* **87,** 217001 (2001).
12. Singley, E. J., Basov, D. N., Kurahashi, K., Uefuji, T. & Yamada, K. Electron dynamics in $Nd_{1.85}Ce_{0.15}CuO_{4+\delta}$: Evidence for the pseudogap state and unconventional *c*-axis response. *Phys. Rev. B* **64,** 224503 (2001).
13. Armitage, N. P. *et al.* Anomalous electronic structure and pseudogap effects in $Nd_{1.85}Ce_{0.15}CuO_4$. *Phys. Rev. Lett.* **87,** 147003 (2001).
14. Renner, Ch., Revaz, B., Genoud, J.-Y., Kadowaki, K. & Fischer, Ø. Pseudogap precursor of the superconducting gap in under- and overdoped $Bi_2Sr_2CaCu_2O_{8+\delta}$. *Phys. Rev. Lett.* **80,** 149–152 (1998).
15. Biswas, A. *et al.* Gapped tunneling spectra in the normal state of $Pr_{2-x}Ce_xCuO_4$. *Phys. Rev. B* **64,** 104519 (2001).
16. Gollnik, F. & Naito, M. Doping dependence of normal- and superconducting-state transport properties of $Nd_{2-x}Ce_xCuO_{4+y}$ thin films. *Phys. Rev. B* **58,** 11734–11752 (1998).
17. Krasnov, V. M., Yurgens, A., Winkler, D., Delsing, P. & Claeson, T. Evidence for coexistence of the superconducting gap and the pseudogap in Bi-2212 from intrinsic tunneling spectroscopy. *Phys. Rev. Lett.* **84,** 5860–5863 (2000).
18. Fournier, P. *et al.* Insulator-metal crossover near optimal doping in $Pr_{2-x}Ce_xCuO_4$: anomalous normal-state low temperature resistivity. *Phys. Rev. Lett.* **81,** 4720–4723 (1998).
19. Ando, Y., Boebinger, G. S., Passner, A., Kimura, T. & Kishio, K. Logarithmic divergence of both in-plane and out-of-plane normal-state resistivities of superconducting $La_{2-x}Sr_xCuO_4$ in the zero-temperature limit. *Phys. Rev. Lett.* **75,** 4662–4665 (1995).
20. Kaminski, A. *et al.* Spontaneous breaking of time-reversal symmetry in the pseudogap state of a high-T_c superconductor. *Nature* **416,** 610--613 (2002).
21. Varma, C. M. Proposal for an experiment to test a theory of high-temperature superconductors. *Phys. Rev. B* **61,** R3804–R3807 (2000).
22. Andergassen, S., Caprara, S., Di Castro, C. & Grilli, M. Anomalous isotopic effect near the charge-ordering quantum criticality. *Phys. Rev. Lett.* **87,** 056401 (2001).
23. Manske, D., Dahm, T. & Bennemann, K.-H. Phase diagram of hole-doped high-T_c superconductors: Effects of Cooper-pair phase fluctuations within fluctuation-exchange theory. *Phys. Rev. B* **64,** 144520 (2001).
24. Lake, B. *et al.* Antiferromagnetic order induced by an applied magnetic field in a high-temperature superconductor. *Nature* **415,** 299–302 (2002).
25. Mook, H. A., Dai, P. & Dogan, F. Observation of magnetic moments in the superconducting state of $YBa_2Cu_3O_{6.6}$. *Phys. Rev. B* **64,** 012502 (2001).
26. Chandra, P., Coleman, P., Mydosh, J. A. & Tripathi, V. Hidden orbital order in the heavy fermion metal URu_2Si_2. *Nature* **417,** 831–834 (2002).
27. Nguyen, H. K. & Chakravarty, S. Effects of magnetic field on the *d*-density-wave order in the cuprates. *Phys. Rev. B* **65,** R180519 (2002).
28. Skinta, J. A., Kim, M.-S., Lemberger, T. R., Greibe, T. & Naito, M. Evidence for a transition in the pairing symmetry of the electron-doped cuprates $La_{2-x}Ce_xCuO_{4-y}$ and $Pr_{2-x}Ce_xCuO_{4-y}$. *Phys. Rev. Lett.* **88,** 207005 (2002).
29. Alff, L. *et al.* Anomalous low temperature behavior of superconducting $Nd_{1.85}Ce_{0.15}CuO_{4-y}$. *Phys. Rev. Lett.* **83,** 2644–2647 (1999).
30. Alff, L. *et al.* Observation of bound surface states in grain-boundary junctions of high-temperature superconductors. *Phys. Rev. B* **58,** 11197–11200 (1998).

Competing interests statement The authors declare that they have no competing financial interests.

Correspondence and requests for materials should be addressed to L.A. (e-mail: lambert.alff@wmi.badw.de).

An inverse transition of magnetic domain patterns in ultrathin films

O. Portmann, A. Vaterlaus & D. Pescia

Laboratorium für Festkörperphysik, Eidgenössische Technische Hochschule Zürich, CH-8093 Zürich, Switzerland

Inverse freezing and inverse melting are processes where a more symmetric phase is found at lower temperatures than at higher temperatures. Such inverse transitions are very rare[1]. Here we report the existence of an inverse transition effect in ultrathin Fe films that are magnetized perpendicular to the film plane. The magnetization of these films is not uniform, but instead manifests itself as stripe domains with opposite perpendicular magnetization[2–4]. Predictions relating to the disordering of this striped ground state in the limit of monolayer film thicknesses are controversial. Mean-field arguments[5–7] predict a continuous reduction of the stripe width when the temperature is increased; other studies[8–11] suggest that topological defects, such as dislocations and disclinations, might penetrate the system and induce geometrical phase transitions. We find, from scanning electron microscopy imaging, that when the temperature is increased, the low-temperature stripe domain structure transforms into a more symmetric, labyrinthine structure. However, at even higher temperatures and before the loss of magnetic order, a re-occurrence of the less symmetric stripe phase is found. Despite the widespread theoretical and experimental work on striped systems, this phase sequence and the microscopic instabilities driving it have not been observed before.

To image the domain structures in face-centred-cubic (f.c.c.) Fe films on Cu(001), we use scanning electron microscopy with polarization analysis (SEMPA; see ref. 12 for details). The black-and-white contrast in the images corresponds to domains of opposite perpendicular magnetization. In order to emphasize details of the images, we sometimes colour white stripes yellow, and dark stripes red or blue. No magnetic field has been applied in this work[12].

The evolution of the domain pattern at room temperature as the film thickness is decreased is shown in Fig. 1a–d. Decreasing the film thickness is equivalent to increasing the effective temperature of the film (Fig. 2). Four distinct patterns can be recognized: a stripe pattern at low effective temperatures, followed by a labyrinthine pattern, a re-entrant stripe domain structure, and finally a contrastless, paramagnetic phase. In Fig. 1e–h the same sequence is observed at a fixed location on a film when the temperature is increased. The inverse freezing process—that is, the transformation from the more symmetric labyrinthine phase to the less symmetric stripe phase—is seen in Fig. 1b, c and Fig. 1f, g. In Fig. 1i–k the temperature is lowered, and again a fixed film location is imaged. The stripe phase (Fig. 1j) emerges from the paramagnetic phase (Fig. 1i) and undergoes inverse melting to a labyrinthine phase (Fig. 1k). This process is extremely slow (Fig. 1k was taken about 12 hours after Fig. 1j). The slow kinetics are probably due to the necessity of rearranging long stripes in a situation of decreasing temperature. Thus, the next transition—from the labyrinthine to the low-temperature stripe phase—is very rare, although occasionally observed (Fig. 1l, m).

In Fig. 2 we report some quantitative aspects of the domain structure. Films grown on substrates held at about room temperature during evaporation have a thickness-dependent Curie temperature T_C (refs 13–15) (here substrate temperature is about 315 K, and deposition rate is about 0.1 monolayers per minute, ML min^{-1}). At low coverages, T_C increases with thickness (Fig. 2a). In this thickness range, decreasing the thickness at constant temperature drives the film towards the phase transition, and is thus equivalent to establishing an increasing effective temperature. After reaching a maximum value, T_C decreases again (Fig. 2a). The value of the maximum and the thickness range for which T_C is above room temperature depend on the growing conditions and on how T_C is determined[13,15,16]. What produces the decrease of T_C is still a controversial point, and is beyond the scope of this Letter.

Mean-field theory[4–7], which does not consider geometrical phase transitions, predicts the width L of the domains to decrease continuously when the temperature or the effective temperature are raised. The stripes assume a finite width L_C at T_C where the magnetization within each stripe vanishes. L_C at T_C was calculated in ref. 6 to be about $4\pi\Gamma/\Omega$, where Γ is a measure of the exchange interaction and Ωa is the strength of the dipolar interaction (here a is the in-plane nearest-neighbour distance). Theoretical work[2,4–6] shows that in a situation of perpendicular magnetization, the value of the magnetic anisotropy does not appear explicitly in the expression for L_C and that L is determined, close to T_C, by the ratio of the exchange to the dipolar interaction. The perpendicular magnetic anisotropy, determined for instance in ref. 17, is a smoothly varying function of the temperature. Setting $a = 0.25$ nm, Γ to $T_C \approx 300$ K and the strength of the dipolar interaction Ωa to $\sim$2.5 K, we calculate $L_C \approx 300$ nm. Figure 2b confirms this value. While imaging from the top to the bottom, the film cools down from the paramagnetic state (top of Fig. 2b), followed by a sudden appearance of stripes with a finite width of $\sim$500 nm. Figure 2c shows that the mean stripe width increases

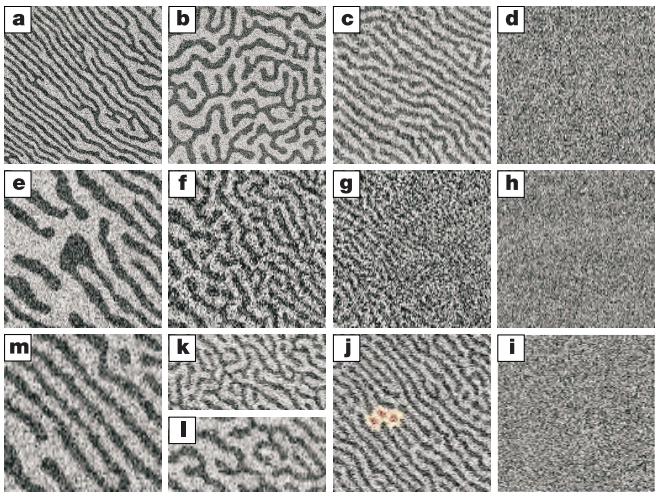

Figure 1 The four phases in ultrathin f.c.c. Fe films. **a**–**d**, The effective temperature is increased from left to right. The paramagnetic phase (**d**) appears contrastless. (By contrastless we mean that the spin polarization averages to zero within 10 ms, which is the measuring time per pixel.) For each image, the image width β and the film parameters δ (thickness) and T (temperature) are given. If not specified, the vertical scale of the images is the same as the horizontal scale. Slightly varying quantities are indicated by the $\approx$ sign. ($\beta_a = 92\,\mu$m, $\beta_b = 46\,\mu$m, $\beta_c = 23\,\mu$m, $\beta_d = 23\,\mu$m, $\delta_a = 2.1$ ML, $\delta_b = 1.91$ ML, $\delta_c = 1.84$ ML, $\delta_d = 1.73$ ML, $T = 293$ K.) **e**–**h**, A fixed region of a film is imaged while the temperature is increased from **e** to **h**. The white stripes in the low-temperature phase are slightly broader than the black stripes: this is due to some residual, unavoidable small magnetic field, as discussed in ref. 6. ($\beta_e = 46\,\mu$m, $\beta_f = 23\,\mu$m, $\beta_g = 23\,\mu$m, $\beta_h = 23\,\mu$m, $\delta \approx 1.89$ ML, $T_e \approx 210$ K, $T_f \approx 268$ K, $T_g \approx 283$ K, $T_h \approx 313$ K.) **i**–**k**, A fixed region of a film is imaged while the temperature is lowered from **i** (paramagnetic phase) to **k** (labyrinthine phase). Notice the bubble-like defects (**j**, red), which are known in pattern formation to be possible precursors of a labyrinthine pattern[23]. ($\beta_i = 23\,\mu$m, $\beta_j = 44\,\mu$m, $\beta_k = 44\,\mu$m, $\delta = 1.97$ ML, $T_i \approx 321$ K, $T_j \approx 300$ K, $T_k \approx 296$ K.) **l**–**m**, The labyrinthine phase transforms into the stripe pattern on cooling. ($\beta_l = 33\,\mu$m, $\beta_m = 33\,\mu$m, $\delta \approx 1.94$ ML, $T_l \approx 294$ K, $T_m \approx 281$ K.)

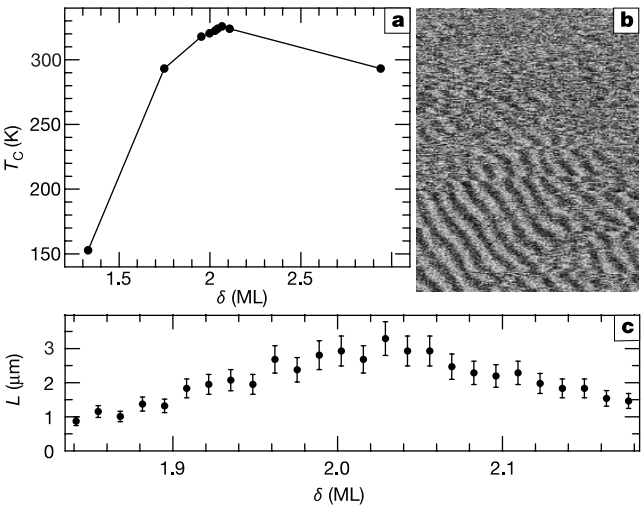

Figure 2 Mean-field aspects of the phase transition. **a**, The phase transition line. Above the line the system is paramagnetic, below it the films are magnetized perpendicular to the film plane. **b**, The finite stripe width at T_C. The film cools down during image taking from the paramagnetic phase (top of the image) to the stripe phase (bottom). ($\beta = 14\,\mu$m, $\delta = 1.94$ ML.) **c**, Mean stripe width at room temperature as a function of the film thickness. The effective temperature is lowest in the centre and increases towards left and right.

smoothly when the effective temperature is lowered, as expected from mean-field arguments. Notice that the maximum of the transition line of Fig. 2a is mirrored in the curve in Fig. 2c, which also undergoes a maximum.

We now look at the role of dislocations. Stripe patterns contain four types of dislocations[12] (shown coloured in Fig. 3a). Most dislocations appear in pairs, possibly separated by one or two continuous stripes: the stripes form the 'smectic-like' phase predicted to develop from the ground state[9–11,18]. The structure factor (inset), obtained by Fourier transformation of the image, has two well-defined spots along one direction in reciprocal space: that is, this stripe phase is orientationally ordered[10]. Imaging the stripes on a wedge (Fig. 3b, the effective temperature increases from left to right) demonstrates the role of dislocations. They allow for new stripes to be inserted (shown coloured) so that the stripe density can increase when T_C is approached, in apparent agreement with mean-field arguments[5]. Notice, however, that this model predicts a continuous adjustment of the stripe width, which is only observed if the mean stripe width is considered.

When the temperature is increased at uniform thickness the dislocations are also seen to glide, the net result being again an increase of the stripe density. This process appears to be forbidden in thick films, which prefer to form a labyrinthine pattern instead[19]. The analogous process of stripe annihilation is shown in Fig. 3c. The stripe pattern is imaged from top to bottom while emerging from the uniform paramagnetic state upon cooling. The three yellow stripes on the top collapse into two by a sudden annihilation process accompanied by a rapid zig-zag movement of the neighbouring stripes (also shown coloured in the figure)—first they move to the left, then back to the right. This movement allows for the adjustment of the change in periodicity produced by stripe annihilation. As thinner stripes merge through a number of discrete steps, the number of stripes within a given field of view is reduced (as can be

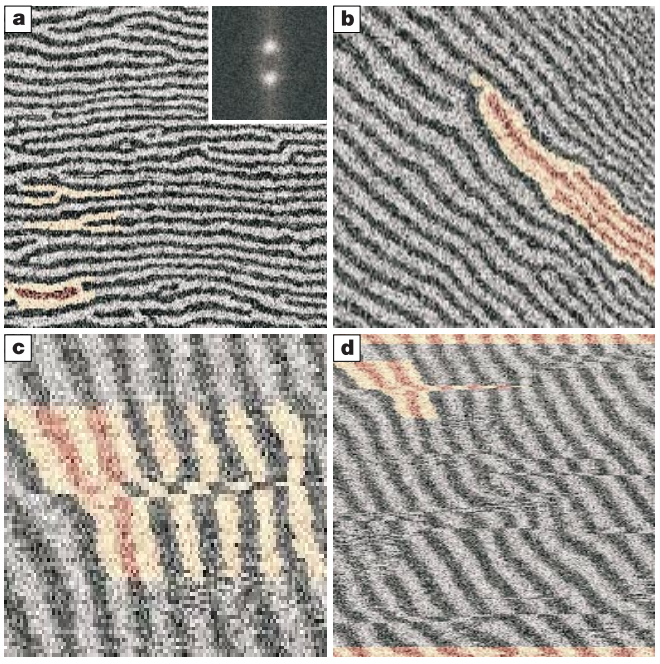

Figure 3 The role of dislocations. **a**, The low-temperature stripe phase, with four types of defects (shown coloured). Inset: structure factor, indicating that the stripes have a local directional order. ($\beta = 46\,\mu$m, $\delta = 2.44$ ML, $T = 293$ K.) **b**, The effective temperature increases from left to right and the stripe density increases by insertion of new stripes (shown coloured). ($\beta = 65\,\mu$m, δ from 2.33 ML to 2.12 ML, $T = 286$ K.) **c**, **d**, The images were taken when the sample was cooling down from the paramagnetic phase to the high-temperature stripe phase. The top of the images has the highest temperature. The stripe density decreases on cooling by annihilation of stripes, followed by the rearrangement of the remaining stripes (shown coloured). ($\beta_c = 12\,\mu$m, (vertical size, 6 μm), $\beta_d = 18.4\,\mu$m, $\delta = 1.96$ ML, $T \approx 295$ K.)

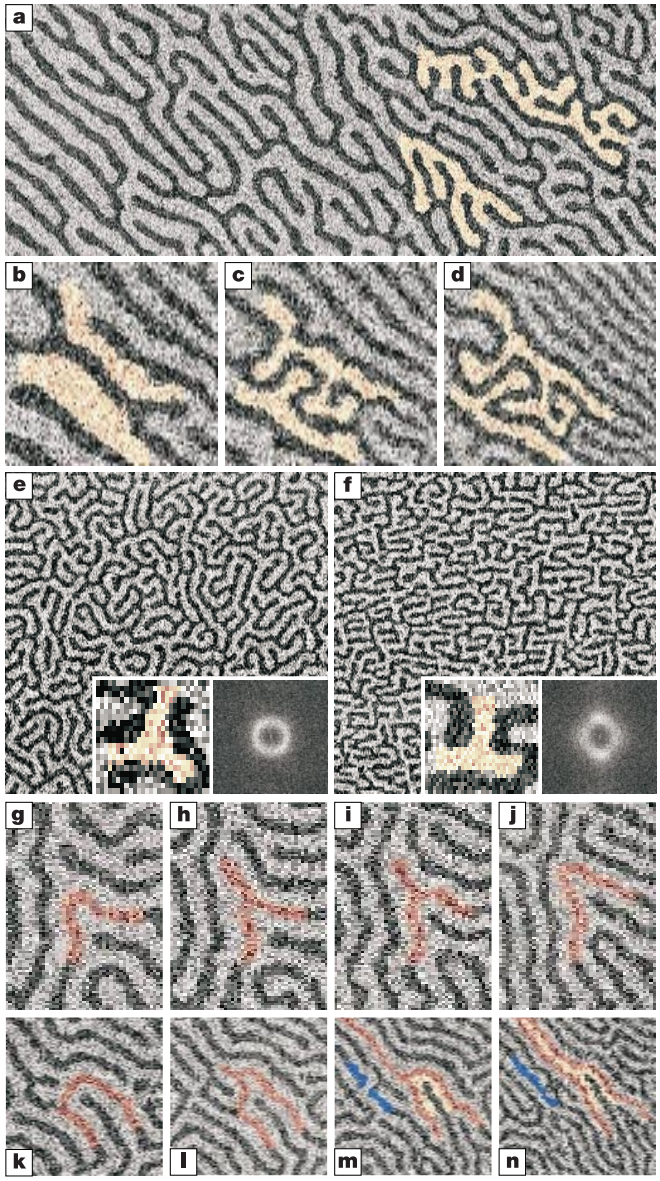

Figure 4 Microscopic mechanisms of transformations. In **a**–**f** the formation of the labyrinthine pattern is illustrated, in **g**–**n** the inverse transformation from a labyrinthine to a high-temperature stripe pattern is imaged. **a**, The effective temperature increases from left to right. The emission of transversal 'fingers' is coloured. ($\beta = 155\,\mu$m, δ varies from 2.06 ML to 1.98 ML, $T = 294$ K.) **b**–**d**, The temperature is increased from left to right for the same film region. The stripes are seen to emit fingers (shown coloured) that wind up to promote the formation of the labyrinthine pattern. ($\beta = 36\,\mu$m, $\delta \approx 2.19$ ML, $T_b \approx 298$ K, $T_c \approx 304$ K and $T_d \approx 305$ K.) **e**, The labyrinthine pattern. The insets show a triangular V-disclination and the structure factor. ($\beta = 92\,\mu$m, $\delta = 1.97$ ML, $T = 293$ K.) **f**, The labyrinthine pattern on a stepped substrate. The disclination has a square symmetry, as does the structure factor. (Parameters as in **e**, $\delta = 2.15$ ML.) **g**–**j** and **k**–**n**, Knee-bend and bridge instabilities (shown coloured) leading to the straightening of the labyrinthine pattern when the temperature is increased (from left to right). ($\beta_{g\text{-}j} = 23\,\mu$m, $\beta_{k\text{-}n} = 33\,\mu$m, $\delta = 1.95$ ML, T is raised from $T_g \approx 311$ K to $T_j \approx 315$ K and from $T_k \approx 311$ K to $T_n \approx 316$ K.)

seen by counting the number of stripes at the top (the 'hot side' of the image) and at the bottom (the 'cold side') of Fig. 3d). Notice that a sudden movement of the sample can be excluded, as stripes not involved in the adjustment are not affected by any discontinuity.

We now consider the microscopic mechanisms of transformations. Figure 4a shows a stripe pattern on a wedge. The effective temperature increases from left to right. The stripes emit fingers and branches transversally to themselves that wind up to initiate orientational melting (some examples are coloured in the figure). The same process is observed when the temperature is increased (Fig. 4b–d). This transversal front instability, predicted in a different context[20], promotes the loss of orientational order in favour of a 'labyrinthine' pattern (Fig. 4e)—a connected network of domains containing two types of defects: convex disclinations (X-type, a domain ending as a tip surrounded by a domain with opposite magnetization looping around it) and concave disclinations (V-type, three segments meeting at one point, see Fig. 4e inset)[21]. A surprising feature is the angle formed by the segments in V-disclinations—predominantly 120°. This local three-fold symmetry can be understood within a planar isotropic system as being due to the repulsive dipolar interaction between segments of the same 'colour', but is in striking contrast to the square symmetry imposed on the lattice by the epitaxial growth on the (100) face, as confirmed by our low-energy electron diffraction images.

The structure factor of the labyrinthine phase (Fig. 4e, inset) has its spectral weight on a ring that is weakly hexagonally shaped, confirming that the orientationally melted state consists of disclinations with three-fold symmetry that have retained a memory of the original stripe orientation. This 'rotational incommensuracy' indicates that the domain structure, residing on a micrometre scale, is totally disjoint from the lattice geometry, residing on $a \approx 0.1$ nm scale. We conclude that the films indeed follow the 'floating solid' hypothesis[5,9–11] formulated for two-dimensional striped systems. The square symmetry is restored when the Fe film is grown on top of a slightly miscut Cu(100) surface. The miscut ($\sim$3°) creates an array of oriented monatomic steps within the substrate (periodicity $\sim$3.5 nm). The stripes in films grown on top of the miscut substrate preferentially align parallel or perpendicular to the steps. The system of oriented monatomic steps does not prevent orientational melting, but the labyrinthine phase emerging from the stripes (Fig. 4f) contains the 90° corners (inset) predicted by theoretical work on a square lattice[9,10]. Accordingly, the spectral weight of the structure factor resides on a square-shaped ring, with maxima at its corners (inset) and resembles the structure factor obtained from Monte Carlo simulations in ref. 10.

These observations clarify the role of the substrate: it provides pinning centres so that the stripe positions are not allowed to fluctuate in time as required for a truly 'floating solid'[5], but does not change the nature of the orientational melting process. This pinning is also essential for selecting locally a direction along which stripes are oriented, although the local direction might vary over large distances, as discussed in ref. 12. In line with the standard model of two-dimensional melting[8,9], we observe the intervening of an intermediate labyrinthine pattern before paramagnetism sets in. Notice, however, that the formation of this intermediate phase is promoted by a transversal front instability of the stripes, and not by a standard decay of dislocations into unbound disclinations[11].

The main microscopic mechanisms of the transition from the labyrinthine pattern to the re-entrant stripe pattern are coloured in Fig. 4g–n. The knee-bend (Fig. 4g, red) emits a segment (Fig. 4h, red) into the adjacent domain of opposite magnetization. The resulting V-disclination opens to a bell-shaped domain (Fig. 4i, red) and transforms into a knee-bend (Fig. 4j, red) again, the main result being the straightening of the original knee-bend area. A similar straightening is produced by a segment emitted by a knee-bend (Fig. 4k–l, red), proceeding into the domain of opposite magnetization and cutting it as a pair of scissors (Fig. 4l, m, red, and Fig. 4m, n, yellow). This mechanism simultaneously allows for the required increase of the stripe density. The emission of segments at knee-bends is reminiscent of the knee-bend instability against formation of VX pairs of disclinations observed as solutions of the Cross-Newell pattern formation equation[21]. Segments are preferentially emitted into one direction, along which the re-entrant stripes align. In a third mechanism, two segments separated by a bridge (Fig. 4m, blue) join into a stripe (Fig. 4n). This mechanism removes dislocations in the re-entrant stripe phase. Reordering neither proceeds via an 'inverted' transversal instability nor via the rebinding of disclinations into dislocations as reported in a similar—although non-two-dimensional melting—labyrinthine-stripe transformation[22].

The present work reports some unpredicted geometrical features of the magnetic phase transition in ultrathin f.c.c. Fe films. These unusual elements should be significant for any type of stripe order, even if it is encountered in a different context, such as the striped quantum liquid crystal phases envisaged recently in connection with copper oxide superconductors[18]. We note that the features reported here are also missing from work on striped quantum liquids. □

Received 23 September 2002; accepted 21 February 2003; doi:10.1038/nature01538.

1. Greer, A. L. Too hot to melt. *Nature* **404,** 134–135 (2000).
2. Garel, T. & Doniach, S. Phase transitions with spontaneous modulation—the dipolar Ising ferromagnet. *Phys. Rev. B* **26,** 325–329 (1982).
3. Seul, M. & Andelman, D. Domain shapes and patterns: the phenomenology of modulated phases. *Science* **267,** 476–483 (1995).
4. Sornette, D. Undulation instability in stripe domain structures of bubble materials. *J. Phys.* **48,** 151–163 (1987).
5. Czech, R. & Villain, J. Instability of two-dimensional Ising ferromagnets with dipole interaction. *J. Phys. Condens. Matter* **1,** 619–627 (1989).
6. Kashuba, A. & Pokrovsky, V. L. Stripe domain structures in a thin ferromagnetic film. *Phys. Rev. B* **48,** 10335–10344 (1993).
7. Gehring, G. A. & Keskin, M. The temperature dependence of the domain spacing in ultrathin magnetic films. *J. Phys. Condens. Matter* **5,** L581–L585 (1993).
8. Nelson, D. R. in *Fundamental Problems in Statistical Mechanics V* (ed. Cohen, E. G. D.) 53–108 (North-Holland, Amsterdam, 1980).
9. Abanov, Ar., Kalatsky, V., Pokrovsky, V. L. & Saslow, W. M. Phase diagram of ultrathin ferromagnetic films with perpendicular anisotropy. *Phys. Rev. B* **51,** 1023–1038 (1995).
10. De'Bell, K., MacIsaac, A. B. & Whitehead, J. P. Dipolar effects in magnetic thin films and quasi-two-dimensional systems. *Rev. Mod. Phys.* **72,** 225–257 (2000).
11. Stoycheva, A. D. & Singer, S. J. Stripe melting in a two-dimensional system with competing interactions. *Phys. Rev. Lett.* **84,** 4657–4660 (2000).
12. Vaterlaus, A. *et al.* Two-step disordering of perpendicularly magnetized ultrathin films. *Phys. Rev. Lett.* **84,** 2247–2250 (2000).
13. Stampanoni, M., Vaterlaus, A., Aeschlimann, M., Meier, F. & Pescia, D. Magnetic properties of thin fcc iron films on Cu(001). *J. Appl. Phys.* **64,** 5321–5324 (1988).
14. Thomassen, J. *et al.* Magnetic live surface layers in Fe/Cu(100). *Phys. Rev. Lett.* **69,** 3831–3834 (1992).
15. Kirilyuk, A., Giergiel, J., Shen, J., Straub, M. & Kirschner, J. Growth of stabilized γ-Fe films and their magnetic properties. *Phys. Rev. B* **54,** 1050–1063 (1996).
16. Man, K. L., Altman, M. S. & Poppa, H. Spin polarized low energy electron microscopy investigations of magnetic transitions in Fe/Cu(100). *Surf. Sci.* **480,** 163–172 (2001).
17. Pierce, J. P., Torija, M. A., Shen, J. & Plummer, E. W. Mapping the magnetic phase diagram of metastable fct Fe/Cu(100) using Co atoms. *Phys. Rev. B* **64,** 224409 (2001).
18. Kivelson, S. A., Fradkin, E. & Emery, V. J. Electronic liquid-crystal phases of a doped Mott insulator. *Nature* **393,** 550–553 (1998).
19. Seul, M. & Wolfe, R. Evolution of disorder in two-dimensional stripe patterns: Smectic instabilities and dislocation unbinding. *Phys. Rev. Lett.* **68,** 2460–2463 (1992).
20. Yochelis, A., Hagberg, A., Meron, E., Lin, A. L. & Swinney, H. L. Development of standing-wave labyrinthine patterns. *SIAM J. Appl. Dyn. Syst.* **1,** 236–247 (2002).
21. Newell, A. C., Passot, T., Bowman, C., Ercolani, N. & Indik, R. Defects are weak and self-dual solutions of the Cross-Newell phase diffusion equation for natural patterns. *Physica D* **97,** 185–205 (1996).
22. Harrison, C. *et al.* Mechanism of ordering in striped patterns. *Science* **290,** 1558–1560 (2000).
23. Pearson, J. E. Complex patterns in a simple system. *Science* **261,** 189–192 (1993).

Acknowledgements We thank the Swiss National Foundation and ETH Zurich for financial support.

Competing interests statement The authors declare that they have no competing financial interests.

Correspondence and requests for materials should be addressed to O.P. (e-mail: portmann@solid.phys.ethz.ch).

